S 2p photoabsorption of the SF_5CF_3 molecule: Experiment, theory and comparison with SF_6

A. Kivimäki [a,*], J. Álvarez-Ruiz [b], M. Coreno [c], M. Stankiewicz [d], G. Fronzoni [e,f], M. Stener [e,f], P. Decleva [e,f]

[a] CNR-IOM, Laboratorio TASC, 34149 Trieste, Italy
[b] Departamento de Química Láser, Instituto de Química-Física Rocasolano, Consejo Superior de Investigaciones Científicas, Serrano 119, 28006 Madrid, Spain
[c] CNR-IMIP, Montelibretti, 00016 Rome, Italy
[d] Instytut Fizyki im. Mariana Smoluchowskiego, Uniwersytet Jagielloński, 30-059 Kraków, Poland
[e] Dipartimento di Scienze Chimiche, Università di Trieste, 34127 Trieste, Italy
[f] INFM DEMOCRITOS and INSTM CRIMSON, Trieste, Italy

ARTICLE INFO

ABSTRACT

The S 2p core excitation spectrum of the SF_5CF_3 molecule has been measured in the total ion yield mode. It resembles a lot the analogous spectrum of SF_6, also recorded in this study, displaying intense transitions to the empty molecular orbitals both below and above the S 2p ionization potential (IP) and weak transitions to the Rydberg orbitals. The S 2p photoabsorption spectra of SF_6 and SF_5CF_3 have been calculated using time-dependent density functional theory, whereby the spin–orbit coupling was included for the transitions below the S 2p IP. The agreement between experiment and theory is good for both molecules, which allows us to assign the main S 2p absorption features in SF_5CF_3.

1. Introduction

Trifluoromethyl sulfur pentafluoride, SF_5CF_3, is a very potent greenhouse gas recently found in the atmosphere [1]. It ranks second, only after SF_6, in terms of the global warming potential (GWP) when calculated over an extended time period of 100 or 500 years [2]. The GWP measures the overall effect of a pulse emission of a gas on the Earth's climate relative to that of the equal mass of CO_2 (GWP = 1). The high GWP of SF_5CF_3 (17,700 over 100 years) results from its large capability to absorb infrared radiation and its long lifetime (800 years [2]) in the atmosphere. Awareness of climatic issues clearly caused an upsurge in the number of spectroscopic studies of the SF_5CF_3 molecule [3]. Remarkably, the S 1s photoabsorption spectrum of this molecule was already reported as early as in 1972 [4]. Photoabsorption studies have recently been performed at all the K-shell edges (C 1s, F 1s and S 1s) [5] and also in the valence region [6] but the sulfur L-shell edges have been overlooked for some reason. Yet the S 2p photoabsorption of SF_5CF_3 may be expected to be particularly interesting, as the closely related SF_6 molecule displays a most spectacular behavior at the S 2p edge: its photoionization cross section shows huge, so-called

shape resonances above the S 2p ionization potential (IP) while pre-edge Rydberg excitations are unusually weak, e.g. [7,8].

These absorption features in SF_6 can be understood by considering the shape of the molecular potential as a function of radial distance from the central S atom [4,9] (a scheme of the potential is presented, for instance, in [8]). The electronegative fluorine ligands help to create a potential barrier in the perimeter of the SF_6 molecule. The potential barrier divides the attractive potential in the inner and outer wells. The core levels are located in the inner well as are also the unoccupied molecular orbitals. The latter can have both negative and positive energies. In the case of positive energy, a quasi-bound state, a shape resonance, is formed. An electron promoted from a core orbital to a shape-resonant state may tunnel through the potential barrier (a very fast process), leaving behind a core-ionized molecule. Decay of the shape-resonant state is therefore considered to be a pure one-electron process. In the potential barrier model, the widths of the shape resonances are mainly caused by the tunnelling time of the trapped photoelectron into the continuum. The core hole lifetime and vibrational excitation upon photoionization constitute additional broadening effects. The wavefunctions of the core orbitals have significant overlaps with those of the empty valence orbitals, resulting in intense structures in the photoabsorption spectrum. The Rydberg orbitals are located in the outer well. Their wavefunctions have only small overlaps with those of the core orbitals, which explains the weak

---

intensities of the corresponding absorption features. A shape resonance can also be regarded as an excitation to an empty molecular orbital embedded in the ionization continuum [10].

The electronic configuration of the SF_6 molecule (O_h point group) has been given, e.g. in [8]. The S 2p atomic orbitals form the triply degenerate $2t_{1u}$ molecular orbital (MO). SF_6 has four virtual valence orbitals: $6a_{1g}$, $6t_{1u}$, which are S–F antibonding, while the low lying S 3d orbitals are split into $2t_{2g}$ and $4e_g$. Dipole selection rules allow excitations from $2t_{1u}$ to $6a_{1g}$, $2t_{2g}$ and $4e_g$, but not to $6t_{1u}$. The S $2p \rightarrow 6a_{1g}$ excitation appears as a bound transition below the S 2p ionization potential (IP), while the S 2p excitations to the $2t_{2g}$ and $4e_g$ virtual orbitals form shape resonances in the photoionization continuum. The S $2p \rightarrow$ Rydberg excitations in SF_6 give rise to rich, but low-intensity structures that converge to the S 2p IPs. They have been analyzed in detail by Hudson et al. [7]. The SF_5CF_3 molecule can be constructed from the SF_6 molecule simply by replacing one F atom in the SF_6 molecule by a CF_3 group. It belongs to the C_s symmetry group, where MOs are of two possible symmetries (a′ and a″) only. The valence electron structure of SF_5CF_3 was studied by photoelectron spectroscopy and quantum chemical calculations by Holland et al. [6], while the same was done for the sulfur L core levels by Kivimäki et al. [11]. The S 2p core orbitals are split into 9a′, 10a′ and 4a″ MOs. The bonding σ(S–C) orbital (29a′) is the highest occupied MO (HOMO) in SF_5CF_3. There are seven virtual valence MOs, followed by other virtual MOs with more Rydberg character. The MO 30a′ corresponds to the lowest unoccupied MO (LUMO), which is σ^* antibonding in character and similar to the σ^* ($6a_{1g}$) antibonding orbital of SF_6. The dipole selection rules in the C_s symmetry group are totally relaxed: both $A′ \rightarrow A″$ and $A′ \rightarrow A′$ transitions are allowed.

The SF_5CF_3 molecule has a cage-like structure that is expected to favour intense molecular excitations at the expense of Rydberg excitations. This has actually been observed in the previously published K-shell photoabsorption spectra of SF_5CF_3 [4,5]. In the present paper, we will investigate the S 2p photoabsorption spectra of the SF_5CF_3 and SF_6 molecules. The spectra look so similar that a tentative assignment of the SF_5CF_3 spectrum could be attempted just by a direct comparison. We have, however, calculated the S 2p photoabsorption spectra of both the molecules using time-dependent density functional theory (TDDFT). The calculations allow us to assign the spectrum of SF_5CF_3 and gain more insight into changes that occur in S 2p photoabsorption when going from SF_6 to SF_5CF_3.

2. Experimental

Measurements were carried out at the Gas Phase Photoemission beamline [12] at the Elettra synchrotron radiation facility, Trieste (Italy). The beamline receives radiation from an undulator in the photon energy range from 14 eV to above 900 eV. Synchrotron radiation is monochromatized by a spherical grating monochromator equipped with a planar pre-mirror. Five interchangeable gratings allow high photon energy resolution to be achieved in the different energy regions of interest.

The S 2p excitation spectrum of SF_5CF_3 was measured in the total ion yield (TIY) mode at the ambient pressure of $\sim 2 \times 10^{-5}$ mbar by recording the ion signal from a microsphere plate (a 1 in. detector from El-Mul Technologies Ltd.). The background pressure of the vacuum chamber without gas was 5×10^{-7} mbar. The TIY of SF_6 was measured for comparison at the pressure of 1.3×10^{-2}ʹmbar using a double ionization cell of Samson type [13]. We will not discuss the experimental intensities of the latter spectrum but its relative intensity ratios reproduce well those in the published photoabsorption spectra [7,14]. The photon energy axis has been calibrated according to the S $2p \rightarrow 6a_{1g}$ and S $2p_{1/2} \rightarrow 2t_{2g}$ excita-

tions as reported in Ref. [7]; for calibration purposes the TIYs of SF_5CF_3 and SF_6 were measured simultaneously as the two experimental vacuum chambers were located each after other along the path of the synchrotron beam. The photon flux was monitored for normalization purposes by recording the ion current from an Au mesh through which the photon beam propagated. The SF_5CF_3 (of purity 99%) and SF_6 (of purity 99.9%) gases were purchased from Apollo Scientific Ltd. and SIAD S.p.A., respectively, and were used as supplied.

3. Theoretical method

Two separate calculations were performed in order to cover the energy regions below and above the S 2p threshold. The first is a bound state TDDFT calculation approach including spin–orbit (SO) coupling within the zeroth-order regular approximation (ZORA) formalism. A SO self-consistent field (SCF) Kohn–Sham (KS) calculation was performed employing a Slater-type orbitals (STO) basis set with the ADF code [15,16]. The KS eigenvalues and orbitals obtained were used as input for the TDDFT calculations. The TDDFT approach for electron excitations and its implementation in the ADF code has been described in detail in the literature [17,18]. In order to extract efficiently core electron excitations, we solve the TDDFT equation over a reduced space of occupied-virtual orbital pairs, where the index of the occupied orbitals is limited to the core orbitals under study (S 2p in the present case) [19,20]. The region above the S 2p threshold of both SF_6 and SF_5CF_3 has been calculated with the continuum TDDFT B-spline linear combination of atomic orbitals (LCAO) method [21], which does not consider the SO coupling. The computational details of the continuum calculations are the same as in Ref. [22], but in the present work only the LB94 exchange correlation (XC) potential [23] has been used.

The basis set employed for the sulfur, fluorine and carbon atoms is the all-electron ZORA basis set for relativistic calculations from the ADF database named QZ4P [24]. The QZ4P ZORA basis set relative to the excited sulphur atom has been further augmented with two shells of diffuse functions, following the even tempered criterion, since Rydberg excited states are involved and diffuse basis functions are necessary to describe transitions towards such states. This set is indicated as (ET-QZ4P-2diff) set.

The adiabatic local density approximation (ALDA) has been used to approximate the XC kernel. For the XC potential the LB94 [25] potential has been used with the ground state (GS) electron configuration. The LB94 potential has been chosen for its correct asymptotic behavior, which is a necessary condition for a good description of high-energy virtual valence orbitals and Rydberg states. We did not employ other functionals such as the statistical average of orbital potential (SAOP) because the previous analysis [22] showed that the LB94 potential represents the best choice for S 2p ionization. The experimental geometries have been employed for both molecules. The present geometry for SF_5CF_3 agrees with that employed in Ref. [6]. This introduces some differences in the labeling of MOs with respect to our previous study [11].

4. Experimental results

Fig. 1 shows the total ion yields of SF_5CF_3 and SF_6 across the S 2p edge. As it can be seen, the spectra are very similar and all the main structures in SF_6 have their counterparts in SF_5CF_3. From lower to higher excitation energies, we observe in both molecules the $6a_{1g}$ resonance, the Rydberg region and the two shape resonances, $2t_{2g}$ and $4e_g$. (Small fluctuations that are barely visible on the $4e_g$ shape resonances of both the molecules are not real structures, but are caused by non-perfect normalization to the photon flux.
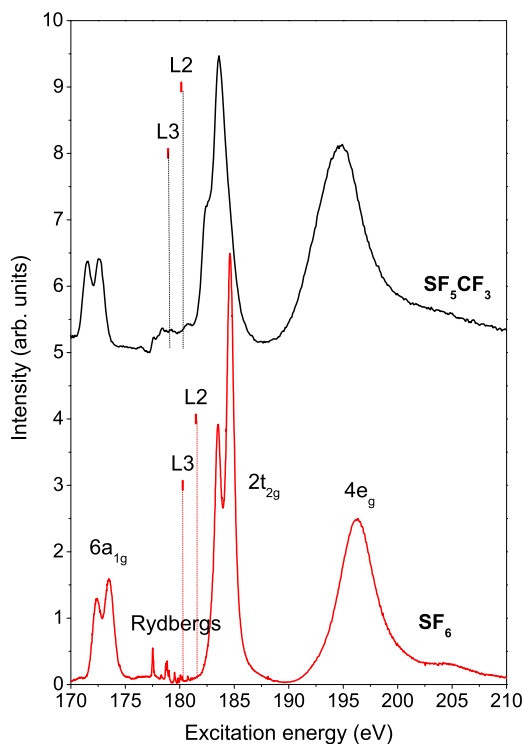
Fig. 1. The total ion yields of SF_6 (bottom) and SF_5CF_3 (top) at the S 2p edge. Some of the known resonances of SF_6 are labeled according to [7]. The $L_{2,3}$ ionization potentials for SF_6 and SF_5CF_3 are from [7,11], respectively. The intensities of the spectra have been scaled approximately so that the $2t_{2g}$ structure in SF_6 and its counterpart in SF_5CF_3 have equal areas. Photon energy resolution at $hv = 180$ eV was ~30 meV in the SF_6 spectrum and ~38 meV in the SF_5CF_3 spectrum.

The latter displayed periodic variations of the order of 2% because the undulator gap was scanned during the experiment.) There are, however, evident differences in the energy positions, spectral shapes and relative intensities between the absorption features in the two molecules. All the molecular resonances in SF_5CF_3 have slightly lower excitation energies than those in SF_6, as can be expected from the chemical shift of 1.35(5) eV observed in the S 2p ionization energies [11]. The S 2p ionization thresholds of SF_5CF_3 were determined to be at 178.92 and 180.13 eV, respectively, using as reference values those of SF_6 at 180.27 and 181.48 eV, as reported by Hudson et al. [7]. Thus the S 2p spin–orbit splitting of 1.21(1) eV is the same for the S 2p ionized states of SF_5CF_3 and SF_6. Note that molecular field (MF) splitting removes the degeneracy of the S $2p_{3/2}$ orbital in SF_5CF_3, caused by the lower symmetry of the molecule. This MF splitting was, however, too small to be observed in [11] (see also calculations in Section 5).

The S 2p photoabsorption spectrum of the SF_6 molecule has been analyzed thoroughly by Hudson et al. [7]. Their spectrum had high resolution (comparable to our spectrum in Fig. 1) and superior statistics even in the region of S 2p-to-Rydberg excitations. We will therefore use the excitation energies given in [7] for the comparison between theory and experiment (see Section 5). In order to obtain more quantitative parameters also for the SF_5CF_3 molecule, its S 2p excitation spectrum was analyzed by a least-squares curve fitting program using Gaussian line profiles. The Rydberg region of the SF_5CF_3 spectrum consists of many overlapping transitions, so some preconditions for parameters were necessary. The spectral intensity was thought to be given by spin–orbit components whose energy separation was fixed in the case of Rydberg excitations to the SO splitting of the S $2p^{-1}$ states, i.e. to 1.21 eV. For excitations to the "$6a_{1g}$" and "$2t_{2g}$" valence orbitals,

the SO splitting was allowed to vary between 1.1 and 1.3 eV. The components of the same SO pair were constrained to have equal widths, the global value of which was, however, allowed to change. The intensity ratios of the spin–orbit components of the core-to-Rydberg excitations were initially fixed to the statistical value of 2:1 for $(S\ 2p_{3/2})^{-1}$:$(S\ 2p_{1/2})^{-1}$, but when such a fit could not reproduce the experimental intensity distribution, this condition was mostly relaxed. In the case of the molecular excitations ("$6a_{1g}$" and "$2t_{2g}$") it is evident from the spectrum that the statistical intensity ratio is not followed. It was not possible to fit the "$2t_{2g}$" shape resonances with two peaks only (like in SF_6), but a second pair of SO lines was needed to get an acceptable fit (see Fig. 2). The energies of the excitations are given in Section 5 together with the theoretical results.

There is a clear peak at 180.65 eV (No. 7′ in Fig. 2) between the S $2p_{1/2}$ threshold and the "$2t_{2g}$" shape resonance. As this peak is within the S 2p continuum, it can not originate from Rydberg excitations. The calculations do not predict any continuum resonance in this energy range (see Section 5). This leads us to conclude that this peak is not associated with a shape resonance but it is most likely due to double excitations that were not included in the calculations. This suggestion can be supported by the following considerations: using experimental energies of the S 2p → LUMO (30a′) core excitations (peaks 1 and 1′ at 171.33 and 172.48 eV, respectively, in Fig. 2) and the shake-up energy of 7.5 eV of the HOMO → LUMO transition in the S 2p photoelectron spectrum [11] one can estimate that the double excited states $2p^{-1}HOMO^{-1}LUMO^2$ are located at ~178.8 and ~180.0 eV. The latter value is quite close to the energy of 180.65 eV observed for the "extra" peak. If its spin–orbit component (No. 7) were located at lower energies, it would occur between the two S 2p IPs, where Rydberg transitions have difficulties to account for all the observed intensity. It can not be extracted from the experimental spectrum how the intensity is divided between the Rydberg transitions and the surmised double excitations in the energy region 178.5–180 eV. A very weak feature (not fitted) that could be due to double excitations is also observed around 186.4 eV in Fig. 2. Their character would be $2p^{-1}HOMO^{-1}LUMO^1Ryd^1$. The energy difference between the double excitation peak 7′ and valence peak 1′ (8.17 eV) gives the energy needed for a HOMO → LUMO shake-up if it accompanies an S 2p → LUMO excitation. Adding this energy to that of the most intense Rydberg excitation (peak 6 at 178.25 eV) one obtains exactly the energy observed. That two continuum features (at 180.65 and 186.4 eV) can be attributed to double excitations in a mutually consistent way gives further credibility to this interpretation.

Apart from the two shape resonances, the S 2p excitation spectrum of SF_6 displays a weak feature at 205 eV (Fig. 1) and a still weaker one at 209 eV [7] in the ionization continuum. The origin of the 205-eV resonance has been contemplated for a long time, e.g. [26], but it is still not clear. Hudson et al. [7] tentatively attributed the two resonances to multielectron excitations, without, however, proposing an exact assignment. The 205-eV structure of SF_6 appears to have its counterpart in the spectrum of SF_5CF_3 at a slightly smaller photon energy (~204 eV). The feature in SF_5CF_3 is wider and it almost seamlessly joins the "$4e_g$" shape resonance.

5. Theoretical results and comparison with experiment

5.1. Bound-state calculations

Fig. 3 reports the S 2p core excitation spectra of SF_6 and SF_5CF_3 calculated at the TDDFT level with the inclusion of the spin–orbit (SO) relativistic effects (ZORA-TDDFT approach). The experimental spectra are reported for comparison. Note that they have been shifted
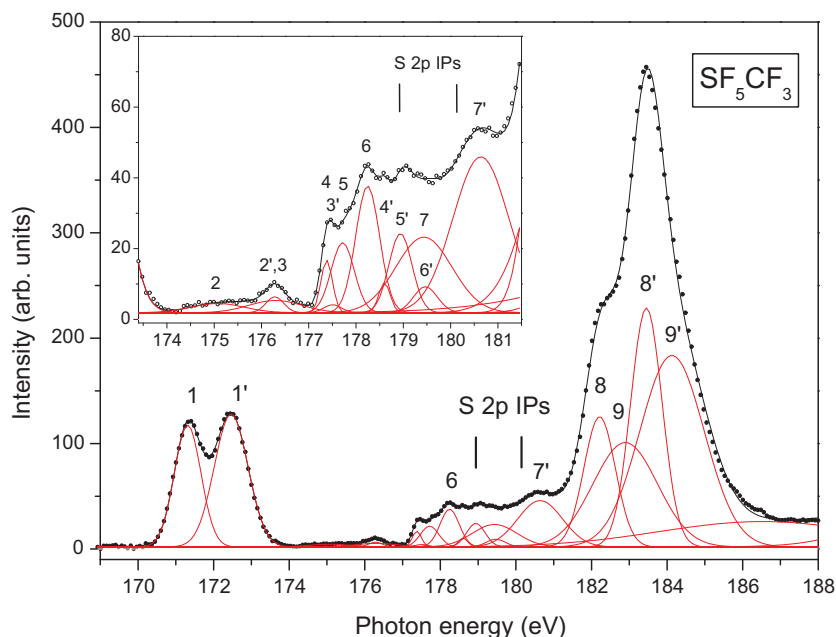
Fig. 2. The decomposition of the S 2p core excitation spectrum of SF_5CF_3 by a Gaussian fit. The inset shows the magnified region of the Rydberg excitations. The S 2p ionization potentials are from [11]. The peaks labeled with same numbers (with and without prime) are spin–orbit components of the same electronic transition.

(by 1 eV) on the calculated energy scale for ease of comparison. Also the transitions calculated above the ionization thresholds (up to about 6 eV above the edge) are included in the figure. These have to be considered with caution because the LCAO-MO approach with a finite basis set can not handle properly the continuum absorption, but it may generate discrete states that are just artifacts of the calculations. The antibonding virtual orbitals are closely associated with the shape resonances observed in the cross section. If the interaction with the non-resonant continuum is rather weak it can be assumed that the high intensity discrete transitions calculated above edge describe approximately the resonant features, at least in the lower energy range. For these two molecules the shape resonances located just above the S 2p IP are correctly described by present bound-state calculations and are therefore included in Fig. 3. The insets show the details of the below-edge spectra, in order to emphasize the Rydberg transitions which are very weak in both molecules. Tables 1 and 2 give the excitation energies of the main structures of SF_6 and SF_5CF_3, respectively. Previous calculations for the S 2p core excitation have been performed for SF_6 [8,27] while no theoretical results are available for SF_5CF_3.

In Tables 1 and 2, we have summarized the calculated excitation energies and oscillator strengths of the below-edge transitions as well as their assignment in terms of the dominant configuration in the final excited state and the sulfur main character of the final MO in that configuration. The calculated S 2p ionization limits are 180.67 (S $2p_{3/2}$) and 181.97 eV (S $2p_{1/2}$) in SF_6 and 179.59 (S $2p_{3/2}$) and 180.89 eV (S $2p_{1/2}$) in SF_5CF_3, with a splitting of 1.30 eV in both molecules. In comparison, the experimental binding energies of the S $2p_{3/2}^{-1}$ states are 0.4 and 0.67 eV lower for SF_6 and SF_5CF_3, respectively, while the observed S 2p SO splitting in both molecules is 1.21 eV [11].

5.1.1. SF_6

Photoabsorption of SF_6 below the S 2p edge is dominated by a doublet structure corresponding to the dipole-allowed excitations to the LUMO ($6a_{1g}$), which is a σ^* antibonding orbital with a significant sulfur 3s contribution (see Table 1). At higher energies very weak Rydberg excitations are present, with characteristically nar-

row linewidths in the experiment. The clear energy separation between valence and Rydberg transitions reflects the lack of mixing between valence and Rydberg components in the calculated excited states. The transitions towards the other two virtual valence levels ($2t_{2g}$ and $4e_g$) give rise to the shape resonances above the S 2p IPs. Only the $2t_{2g}$ shape resonance, which lies just above the threshold, is shown in Fig. 3. The doublet structure of the valence features ($6a_{1g}$ and $2t_{2g}$) derives from the SO interaction which splits the sulfur 2p core hole into the $2p_{3/2}$ and $2p_{1/2}$ levels. The calculated SO splitting of the S 2p → $6a_{1g}$ excitations (peaks 1 and 2 in Fig. 3) is 1.22 eV, in excellent agreement with the experimental value (1.17 eV [7]). The more intense doublet just above the threshold (peaks 3 and 4 in Fig. 3, not included in Table 1) is assigned to the promotion of the S 2p electron to the quasi-bound $2t_{2g}$ orbital with an SO splitting again of 1.22 eV. Note that the intensity ratio of the SO components is close to unity for the $6a_{1g}$ resonance and less than unity for the $2t_{2g}$ resonance, thus deviating considerably from the statistical ratio of $(2p_{3/2})^{-1}:(2p_{1/2})^{-1} = 2:1$. This trend of the intensity ratio has been explained as an effect of exchange interaction between the 2p core hole and the excited electron [4,7] and can not be described within the one-particle theories. Approaches that go beyond the ground state are needed, such as the present ZORA-TDDFT method which is capable of including both configuration mixing and SO coupling and can give a quantitative description of the L-edge spectra of molecules [25,28].

Between the $6a_{1g}$ and $2t_{2g}$ features several weak lines are calculated which correspond to electron excitations toward Rydberg-type MOs of atomic sulfur character. The experiment shows a richer and more complex structure in this region due to the overlapping manifolds of peaks deriving from vibrational excitations (not included in the present calculations), which renders a comparison with the theoretical results more difficult. The calculated lines are grouped in four peaks labeled a to e in Fig. 3 and Table 1. The first and most intense Rydberg excitations are towards the sulfur 4s orbital from both the $2p_{3/2}$ and $2p_{1/2}$ core levels which give rise to the a and b structures split by about 1.29 eV, in good agreement with previous experimental attribution [7]. Peaks d and c are assigned to the SO components of the sulfur 3d Rydberg transitions,
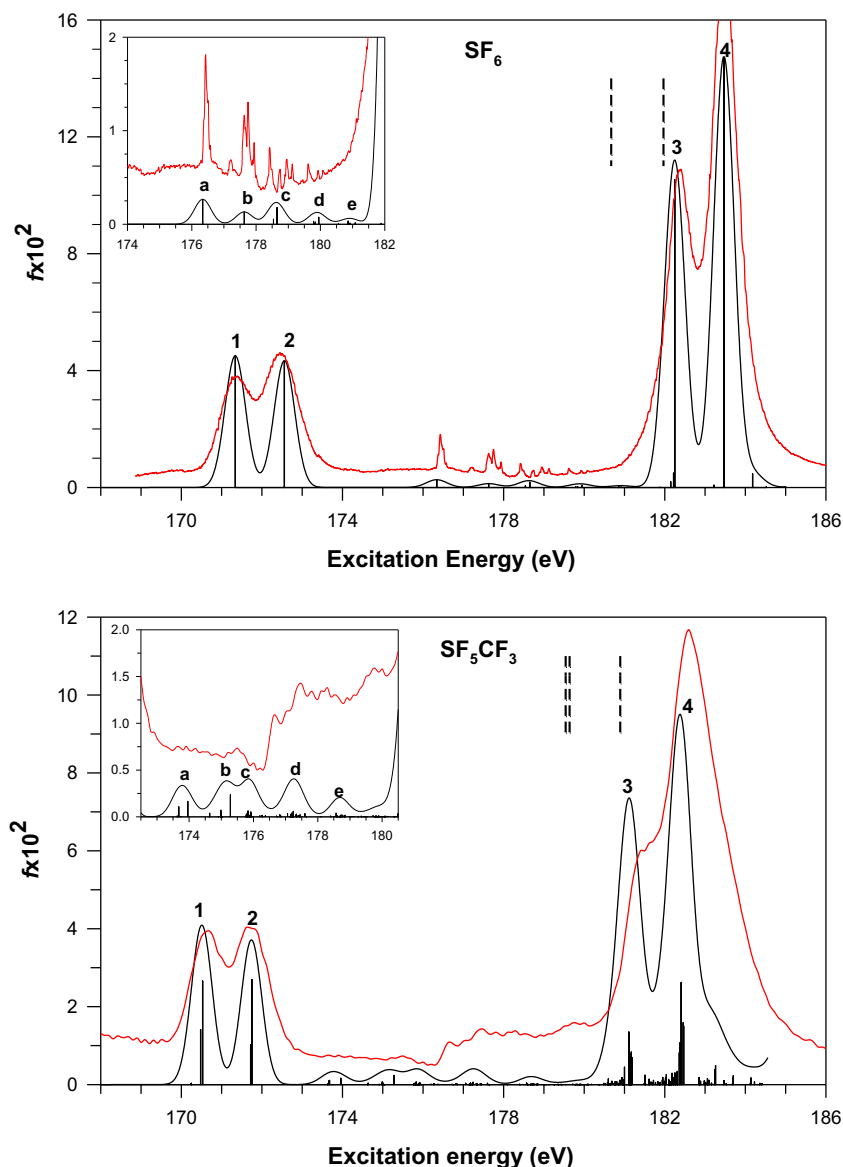
Fig. 3. The black solid curves show the S 2p excitation spectra of the SF$_6$ (upper panel) and SF$_5$CF$_3$ (lower panel) molecules calculated using the ZORA-TDDFT approach that incorporates spin–orbit coupling. The calculated transitions, depicted with bars, are convoluted with Gaussian functions of FWHM = 0.6 eV. The dashed bars denote the calculated L$_{2,3}$ ionization limits. The experimental spectra (red curves) have been shifted by 1 eV to lower photon energies in order to facilitate comparison. The insets show the magnifications of the Rydberg regions. (For interpretation of the references to color in this figure legend, the reader is referred to the web version of this article.)

with a splitting of about 1.30 eV again in accord with the experiment (1.20 eV [7]). The lines contributing to each peak derive from the multiplet splitting of the sulfur 3d orbitals in the octahedral symmetry of SF$_6$. The calculated energy splitting of 3dt$_{2g}$ and 3d$_{eg}$ transitions is about 0.1 eV for both the two SO components. The next d Rydberg series contributes to peak e; the intensity of these lines is lower and refer to the 2p$_{3/2}$ component while the lines of the 2p$_{1/2}$ component are pushed above the 2p$_{3/2}$ threshold.

5.1.2. SF$_5$CF$_3$

The shape of the calculated SF$_5$CF$_3$ spectrum is quite similar to that of SF$_6$ with the dominating two-peaked valence features, one at the lowest excitation energy and the other just above S 2p threshold, separated by a Rydberg region of low intensity (see Fig. 3). A shift to lower energy of about 1.3 eV is observed for the SF$_5$CF$_3$ structures with respect to those of SF$_6$. This is caused by the replacement of a F ligand by a less electronegative CF$_3$ ligand. A closer inspection of the calculated profiles reveals a much more

complex situation than in SF$_6$, with a very large number of lines contributing to the spectral features. In the SO relativistic description, the S 2p orbitals in the C$_s$ symmetry of the molecule correspond to three spinors which are described by a mixing of the 2p$_x$ (a′), 2p$_y$ (a′) and 2p$_z$ (a″) non-relativistic point group components. The two spinors of the L$_3$ (2p$_{3/2}$) component are not degenerate but are split by about 0.1 eV (molecular field splitting), while their separation from the third spinor of the L$_2$ component (2p$_{1/2}$) is 1.3 eV (SO splitting). Transitions can start from each of these three spinors and two final excited states of A′ and A″ symmetry are allowed for the total electronic wavefunction. The excited states converge towards three ionization thresholds, two S 2p$_{3/2}$ thresholds and one S 2p$_{1/2}$ threshold. The intensity distribution among the final excited states is also modulated by the configuration mixing included in the TDDFT scheme.

The first structure in the calculated spectrum is assigned to the excitation of the core electron to the LUMO orbital (30 a′) with the SO splitting accounting for the double-peaked structure. The SO

Table 1
Experimental and calculated excitation energies (eV) and oscillator strengths f for the S 2p excitation spectrum of SF_6[f]. Peak labels refer to those used in Fig. 3.

Exp. energy [7]	Assignment [7]	Peak	Calc. E (eV)	$f \times 10^{2g}$	Final state transition/dominant S character of final MO
172.27	$6a_{1g}$ ($2p_{3/2}$)	1	171.34	4.506	$2p_{3/2} \rightarrow 6a_{1g}/3s$
173.44	$6a_{1g}$ ($2p_{1/2}$)	2	172.56	4.338	$2p_{1/2} \rightarrow 6a_{1g}$
177.42	$4s(2p_{3/2})$	a	176.34	0.267	$2p_{3/2} \rightarrow 7a_{1g}/4s$
178.21	$4p$ ($2p_{3/2}$)				
178.63	$4s(2p_{1/2})$	b	177.63	0.132	$2p_{1/2} \rightarrow 7a_{1g}/4s$
178.76	$3d(2p_{3/2})$				
179.44	$4d$	c	178.54	0.054	$2p_{3/2} \rightarrow 4e_g/3d$
179.74	$5d$		178.65	0.180	$2p_{3/2} \rightarrow 2t_{2g}/3d$
178.95	$5s$ ($2p_{3/2}$)				
179.50	$6s$ ($2p_{3/2}$)				
179.96	$3d$ ($2p_{1/2}$)				
180.00	$3d$ ($2p_{1/2}$)				
180.64	$4d$	d	179.79	0.030	$2p_{3/2} \rightarrow 8a_{1g}/4s$, ns
180.94	$5d$		179.84	0.024	$2p_{1/2} \rightarrow 4e_g/3d$
			179.95	0.075	$2p_{1/2} \rightarrow 2t_{2g}$
		e	180.86	0.036	$2p_{3/2} \rightarrow 3t_{2g}/3d$, 4d
			180.92	0.012	$2p_{3/2} \rightarrow 5e_g/4d$
			181.08	0.015	$2p_{1/2} \rightarrow 8a_{1g}$
				Cross Section (Mb)	
183.40	$2t_{2g}$ ($2p_{3/2}$)		183.5[h]	26.7 [h]	$2p \rightarrow 2t_{2g}$
184.57	$2t_{2g}$ ($2p_{1/2}$)				
196.2	$4e_g$		197.0[h]	19.2[h]	$2p \rightarrow 4e_g$

[f] Calculated two-components DFT-KS S2p ionization limits are 180.67 eV ($2p_{3/2}$) and 181.97 eV ($2p_{1/2}$). Experimental values: 180.27 eV and 181.48 eV [7].

[g] Calculated transitions with $f \times 10^2 > 0.010$ are reported.

[h] From calculations above threshold.

splitting is 1.23 eV, in good accord with the experimental value (1.15 eV) and the value calculated for SF_6. The calculated intensity ratio of the two peaks is close to unity, reproducing the behavior already discussed for SF_6, whereas the experimental intensity ratio, taken from the areas of the peaks, is 0.88. The fit of the experimental spectrum (Fig. 2) yields that the S $2p_{3/2}$ component is narrower than the S $2p_{1/2}$ component (0.83 eV vs. 1.05 eV). A similar observation has been made for the S $2p \rightarrow 6a_{1g}$ excitations in SF_6 [7]. Around 174 eV, transitions are calculated to valence virtual orbitals with partial σ^* (S–C) character, which gives rise to peak a and also contributes to peak b in the theoretical spectrum (see Fig. 3 and Table 2). They are significantly weaker than the main peaks because of the dominant S 3p character in the final MOs. We assign the very weak and rather wide features 2 (at ~175.1 eV) and 2′ (at ~176.3 eV) in the experimental spectrum (Fig. 2) to these valence excitations. The corresponding virtual valence transitions are symmetry-forbidden in SF_6 in which the virtual allowed MOs between the LUMO and S 2p IPs have pure Rydberg character and are well separated in energy from the valence excitations.

The following virtual MO (32 a′) has a predominant 4s sulfur character; however, some S 3p valence character is still present. The mixing between the valence and Rydberg components prevents a simple classification of the final states and tends to distribute the oscillator strength among many excitations. The Rydberg 4s sulfur component is present in several MOs and the relative transitions contribute to peak b ($2p_{3/2}$ component) and c ($2p_{1/2}$ component) with an SO splitting of about 1.3 eV. The experiment displays the first excitation of probable Rydberg character at 176.30 eV (peak 3 in Fig. 2). We assign it to the 4s Rydberg states, even though its term value (= energy difference from the S $2p_{3/2}$ IP) of 2.62 eV is somewhat smaller than that of 2.85 eV observed for the analogous transitions in the SF_6 molecule [7]. Peak 3 is separated from other Rydberg peaks by a short region of negligible spectral intensity. The next Rydberg excitation (4) has a narrow width, as judged by its rising edge. Its term value is 1.53 eV, which is similar to those of the S $2p_{3/2} \rightarrow 3d$ transitions (term value

1.49 eV) in SF_6 [7]. This assignment also agrees with the calculation that attributes peaks d and e to the two SO components of the sulfur 3d Rydberg transitions. The detailed comparison of this energy region with the experiment is only qualitative due to the lack in the theoretical approach of vibrational excitations, which are probably responsible for the richer structure present in the experimental spectrum, as in the case of SF_6. The experimental spectrum of SF_5CF_3 also shows rather clear maxima at 178.26 and 178.94 eV (peaks 6 and 5′ in Fig. 2) but their term values do not coincide with those found in SF_6.

The most intense doublet just above threshold (peaks 3 and 4 in Fig. 3) corresponds to the SO components of the S 2p excitation to a quasi-bound orbital of predominant 3d sulfur character, very similar to the $2t_{2g}$ shape resonance in SF_6. The bound-state calculations do not account for the peak observed in the experiment at 180.65 eV, just above the S$2p_{3/2}$ threshold. This leads us to exclude that this peak would be associated to a shape resonance.

It is interesting to note that in SF_6 several transitions, which are forbidden under strict dipole selection rules become prominent in electron scattering under non dipolar conditions [29,30]. In the S 2p excitation spectrum those transitions are associated with the $6t_{1u}$ valence virtual orbital. They actually appear very weakly in photoabsorption [7], but become formally dipole allowed in the reduced C_s symmetry of SF_5CF_3. However, in the calculation it is observed that such transitions are all very weak, indicating that the symmetry breaking around the sulphur atom, and therefore the S 2s/S 2p mixing in the MOs, is a minor effect.

5.2. Calculations for continuum resonances

In the upper panel of Fig. 4, the calculated photoabsorption above the S 2p edges of SF_6 and SF_5CF_3 is considered. Both profiles are characterised by two very pronounced features, whose nature, at least for SF_6, is well known since the original works of Nefedov [9] and Dehmer [4] who attributed both structures to shape resonances corresponding to excitations of the S 2p core electron to

Table 2
Calculated excitation energies (eV) and oscillator strengths f for S 2p photoabsorption of SF$_5$CF$_3$[f]. Experimental energies (with accuracy of ±0.15 eV) are from the fit shown in Fig. 2. Experimental peak numbers refers to Fig. 2 and theoretical peak labels to Fig. 3.

Exp. E (eV)	Peak No. (Assignm.)	Peak	Calc. E (eV)	$f \times 10^{2}$[g]	Final State transition/dominant S character of final MO
171.33	1 ($2p_{3/2} \to$ "$6a_{1g}$")	1	170.48	1.414	$2p_{3/2} \to 30a'/3s$
			170.53	2.658	$2p_{3/2} \to 30a'$
172.48	1' ($2p_{1/2} \to$ "$6a_{1g}$")	2	171.72	1.019	$2p_{1/2} \to 30a'$
			171.75	2.700	$2p_{1/2} \to 30a'$
175.09	2 ($2p_{3/2} \to$ "$6t_{1u}$")	a	173.67	0.102	$2p_{3/2} \to 31\ a'/3p + 2p_{3/2} \to 19a''/3p$
			173.68	0.107	$2p_{3/2} \to 19a''$
			173.96	0.164	$2p_{3/2} \to 19a''$
176.30	3 ($2p_{3/2} \to$ 4s Ryd)	b	174.64	0.040	$2p_{3/2} \to 32a'/4s$
			174.98	0.033	$2p_{1/2} \to 31a'$
			174.99	0.071	$2p_{1/2} \to 31a' + 2p_{3/2} \to 33a'/4s + np$
176.30	2' ($2p_{1/2} \to$ "$6t_{1u}$")		175.00	0.073	$2p_{1/2} \to 19a''$
			175.28	0.235	$2p_{1/2} \to 31a' + 2p_{3/2} \to 33a'$
		c	175.83	0.121	$2p_{3/2} \to (35a'/4s\ S, np + 20a''/np)$ [h]
			175.91	0.050	$2p_{3/2} \to 35a' + 2p_{1/2} \to 32a'$
177.51	3' ($2p_{1/2} \to$ 4s Ryd)		175.92	0.053	$2p_{1/2} \to 32a'$
		d	177.18	0.060	$2p_{1/2} \to (35a' + 20a'')$ [h]
177.39	4 ($2p_{3/2} \to$ 3d Ryd)		177.24	0.108	$2p_{3/2} \to 22a''/3d + 2p_{3/2} \to 39a'/3d$
			177.32	0.047	$2p_{3/2} \to 22a''/3d, nd$
			177.42	0.036	$2p_{3/2} \to 23a''/3d, nd$
			177.45	0.038	$2p_{3/2} \to 40a'/3d, nd$
			177.60	0.035	$2p_{1/2} \to 21a''$
177.73	5 ($2p_{3/2} \to$ Ryd + vib)				
178.26	6 ($2p_{3/2} \to$ high Ryd)				
178.50	4' ($2p_{1/2} \to$ 3d Ryd)	e	178.57	0.041	$2p_{1/2} \to 39a'/3d$
			178.59	0.012	$2p_{1/2} \to 22a''$
			178.71	0.026	$2p_{1/2} \to 40a'$
			178.75	0.022	$2p_{3/2} \to 25a''/nd$
178.94	5' ($2p_{1/2} \to$ Ryd + vib)				
179.47	6' ($2p_{1/2} \to$ high Ryd)				
179.45	7 ($2p_{3/2} \to$ d.exc)				
180.65	7' ($2p_{1/2} \to$ d.exc)			Cross sect. (Mb)	
182.23	8 ($2p_{3/2} \to$ "$2t_{2g}$")		182.6[i]	19.3[i]	$2p \to 2t_{2g}$
182.90	9 ($2p_{3/2} \to$ "$2t_{2g}$")				
183.47	8' ($2p_{1/2} \to$ "$2t_{2g}$")				
184.15	9' ($2p_{1/2} \to$ "$2t_{2g}$")				
194.8	$2p \to$ "$4e_g$"		195.6[i]	14.5[i]	$2p \to 4e_g$

[f] Calculated relativistic DFT-KS S 2p ionization limits are 179.64 and 179.54 eV ($2p_{3/2}$) (L$_3$ edge) and 180.89 eV ($2p_{1/2}$) (L$_2$ edge). Experimental values: 178.92, 180.13 eV [11].
[g] Calculated transitions with fx10^2 > 0.010 are reported.
[h] These transitions are towards final spinors described as a mixing of virtual non-relativistic MOs, indicated in parenthesis.
[i] from calculations above threshold.

quasi-bound valence virtual orbitals above the ionization threshold. These orbitals derive from the atomic S 3d orbitals, split by the octahedral molecular field of SF$_6$. The shapes of such unbound orbitals can be profitably described by employing the dipole-prepared continuum orbitals [31]. For SF$_6$ they have been already analyzed (see the two upper panels of Fig. 3 in Ref. [22]), confirming the d_{xy}, d_{xz}, d_{yz} nature of the $2t_{2g}$ resonant continuum and the $d_{x_2-y_2}$, d_{z_2} nature of the $4e_g$ resonant continuum. From such an analysis, also the strong σ^*(S–F) antibonding interaction between the S 3d atomic function and the F lone pairs present in the $4e_g$ resonant continuum is evident, explaining the large energy gap observed between the two spectral features.

The calculated profiles for SF$_6$ and SF$_5$CF$_3$ do not show large differences; the most evident effect is the shift of the SF$_5$CF$_3$ profile to a lower energy than that of SF$_6$, and, more interestingly, the pronounced broadening of the $4e_g$ feature. The broadening is evident also in the experimental spectra (Fig. 1). In order to give a quantitative assessment of the spectral differences between the two molecules, we have collected the calculated photon energy and intensity values in Tables 1 and 2. The energy shift of the whole photoabsorption profile between SF$_6$ and SF$_5$CF$_3$ can be assessed from the energy shifts of the $2t_{2g}$ and $4e_g$ shape resonances, which are calculated to be 0.9 eV and 1.4 eV, respectively, in excellent agreement with the experimental shifts (1.1 eV for $2t_{2g}$ – using

the energy of peak 8' in Fig. 2 – and 1.4 eV for $4e_g$). These values are very close to the S 2p binding energy difference between the two molecules, which is 1.35 eV [11], so we can attribute the energy shift in the profiles mainly to the chemical shift. Since the continuum calculation does not include SO coupling, the t_{2g} resonance is not split, as instead was obtained in the bound state calculation.

The broadening of the $4e_g$ shape resonance in SF$_5$CF$_3$ is analyzed in detail in the lower panel of Fig. 4, where S 2p photoabsorption of SF$_5$CF$_3$ has been split according to the three Cartesian components of the S 2p orbitals: the orbital 10a' corresponds to the S 2p orbital directed along the S–C bond. From the figure it is evident that the broader '$4e_g$' shape resonance of SF$_5$CF$_3$ is a consequence of a molecular field effect on the $4e_g$ quasi-bound state: the 10a' component is located almost 2 eV below the other two components (9a' and 4a''). It is worth noting that the MF splitting of the S 2p orbitals is about 0.1 eV, so the calculated splitting must be attributed to the MF splitting of the $4e_g$ quasi-bound state, which splits because the symmetry is reduced and because the electron repulsion effect of the CF$_3$ moiety is less pronounced than that of the F ligand. It is convenient to rationalize this effect by assuming the S–C bond along the x-axis: the 10a' MO then corresponds to 2p$_x$, while 9a' and 4a'' correspond to the pair 2p$_y$ and 2p$_z$. From atomic dipole selection rule, upon ionization from 2p$_x$ only the $3d_{x_2-y_2}$
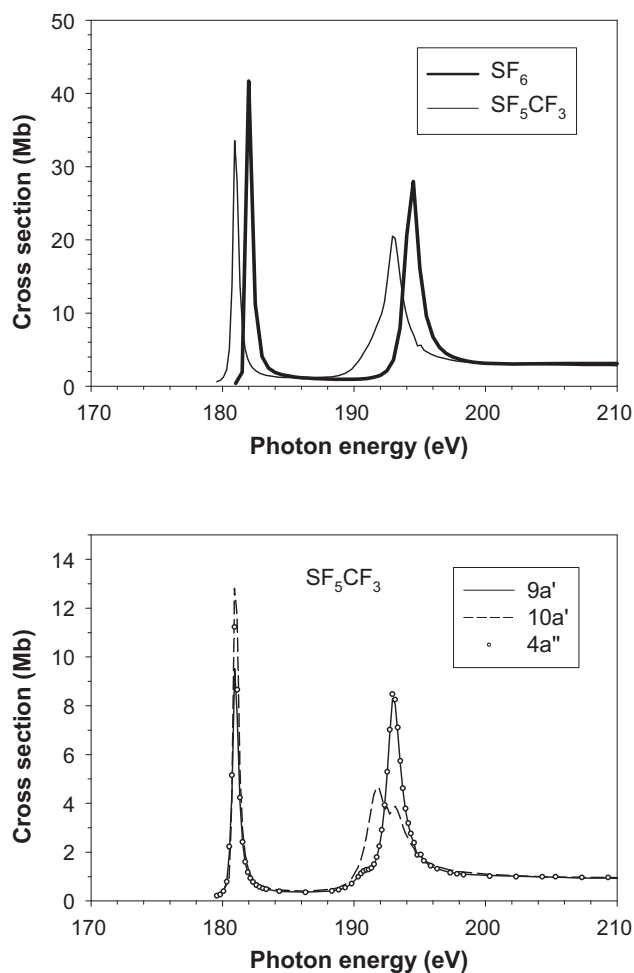
Fig. 4. (upper panel) The photoabsorption cross sections of the SF_6 and SF_5CF_3 molecules above the S 2p edges calculated using the continuum TDDFT B-spline LCAO method. (lower panel) The photoabsorption contributions shown separately for the three different S 2p hole states of SF_5CF_3.

component of the $4e_g$ will be reached, while starting from $2p_y$ or $2p_z$ both $3d_{x_2-y_2}$ and $3d_{z_2}$ are allowed. Therefore the calculated shift of 2 eV between $10a'$ component and $9a'$, $4a''$ components must be attributed to the splitting of the virtual valence $4e_g$ manifold in its $3d_{z_2}$ and $3d_{x_2-y_2}$ components. On the other hand, the $2t_{2g}$ shape resonance does not show any appreciable splitting, which is a consequence of the different localization of the photoelectron wavefunction. The dipole-prepared continuum orbitals in SF_6 do not point towards the ligands, but rather follow diagonal directions and are therefore less sensitive to changes in the nature of the ligands.

It should be noted that the $4e_g$ resonance of SF_6 exhibits effects that cannot be explained by the simple shape resonance model. In a photoelectron study, Ferrett et al. [26] observed that the intensities of both the S 2p main photoelectron lines and the lowest-energy S 2p shake-up satellite line are enhanced at the $4e_g$ resonance. The behavior of the satellite peak contradicts with the interpretation of the $4e_g$ shape resonance as a one-electron effect. Consequently, Ferrett et al. [26] presented that the $4e_g$ resonance has some multielectron character, resulting either from the coupling between the continuum channels (i.e. between S 2p single-hole ionization and S2p ionization with shake-up excitation) or from the coupling of doubly excited states with the S 2p photoionization channel. Photodissociation studies [32,33] have provided further support to the contribution of multielectron transitions at the $4e_g$ reso-

nance. It is likely that the "$4e_g$" shape resonance of the SF_5CF_3 molecule also exhibits multielectron effects, since S 2p electron transitions in these two molecules are generally quite similar. Such effects have not yet been verified experimentally.

We do not observe in the calculations any feature of appreciable intensity near the threshold. This excludes the attribution of the experimental structure found at 180.65 eV to a shape resonance, but rather corroborates its assignment to a double electron excitation. A comparison between experiment (Fig. 1) and theory shows a good agreement for the energies of the resonant maxima. The "$4e_g$" resonance of SF_5CF_3 does not appear structured in photoabsorption, in contrast to the theoretical cross section. The predicted structure may be obscured by the large widths of the shape-resonant states. As noticed also for SF_6, the calculated width of the resonance is significantly narrower than the experimental one. Several factors contribute to that. The broadening effects due to instrumental resolution, core hole lifetime width and vibrational excitations are not taken into account in the theoretical profile, but these factors only amount to few tenths of an eV, as can be estimated from the experimental widths of the S 2p photoelectron lines [11]. The neglect of the S 2p SO splitting reduces more significantly (by ~1 eV) the width of the theoretical profile, but it is likely that the underestimation of the resonant width is a sign of a deficiency in the V_{XC} potential employed in the present study. Some broadening factors may also differ for the S $2p_{1/2}$ and S $2p_{3/2}$ holes. Indeed, it has been observed that the S $2p_{1/2}$ and S $2p_{3/2}$ single-hole photoionization cross sections display different behaviors at the $4e_g$ shape resonance: the S $2p_{3/2}$ photoionization experiences a wider shape resonance than the S $2p_{1/2}$ photoionization [11]. This is at least in a qualitative agreement with the present calculation. However, the S $2p_j$ ($j = 1/2, 3/2$) photoionization cross sections also have different widths at the $4e_g$ shape resonance in SF_6 [34] in which the $4e_g$ orbital is not split by the molecular field. Finally, the fit of the experimental spectrum (Fig. 2) hints that there is an additional (other than SO) splitting at the $2t_{2g}$ shape resonance in SF_5CF_3, which is not explained by either calculation.

6. Conclusions

The S 2p core excitations in the SF_6 and SF_5CF_3 molecules have been studied experimentally and theoretically. The S 2p photoabsorption spectrum of SF_6 is well known for intense excitations to the valence-type MOs, two of which form shape resonances above the S 2p IP. The S 2p core excitation spectrum of SF_5CF_3 has an appearance very similar to that of SF_6. The below-edge transitions were calculated for both molecules using time-dependent density functional theory with the inclusion of spin–orbit splitting (ZORA-TDDFT approach). This level of theory can reproduce well the intensity ratios between the SO components of the valence excitations that deviate significantly from the statistical ratio of 2:1 for $(S2p_{3/2})^{-1}$:$(S2p_{1/2})^{-1}$. The S 2p excitations to Rydberg orbitals gain little intensity in these molecules. They are well resolved in SF_6, and have been assigned previously [7], but form a rather continuous intensity distribution in SF_5CF_3 due to many overlapping electronic transitions that are broadened by vibrational excitations. Nevertheless, a partial assignment of the S 2p → Rydberg excitations in SF_5CF_3 has been achieved with the aid of theory and through comparison with SF_6. A photoabsorption feature, which is not predicted by theory, is observed immediately above the S 2p threshold. It has been tentatively assigned to double excitations.

The photoabsorption spectra of SF_6 and SF_5CF_3 above the S 2p edges were calculated with the continuum TDDFT B-spline LCAO method which does not include SO coupling. The energies of the

shape resonances are correctly predicted: the change in their positions in going from SF_6 to SF_5CF_3 can mostly be attributed to the chemical shift of the S 2p binding energies. The calculated profiles are narrower than the experimental ones, but the calculation predicts the broadening of the $4e_g$ resonance in SF_5CF_3 as compared to that of SF_6, which is also observed in the experiment. The effect is attributed to the splitting of the continuum "$4e_g$" resonance in the molecular field of SF_5CF_3.

Acknowledgements

References

[1] W.T. Sturges, T.J. Wallington, M.D. Hurley, K.P. Shine, K. Sihra, A. Engel, D.E. Oram, S.A. Penkett, R. Mulvaney, C.A.M. Brenninkmeijer, Science 289 (2000) 611.
[2] P. Forster et al., Changes in atmospheric constituents and in radiative forcing, in: Climate Change 2007: The Physical Science Basis, Cambridge Univ. Press, Cambridge UK and New York, NY, USA.
[3] R.P. Tuckett, Adv. Fluorine Sci. 1 (2006) 89. and references therein.
[4] J.L. Dehmer, J. Chem. Phys. 56 (1972) 4496.
[5] T. Ibuki, Y. Shimada, S. Nagaoka, A. Fujii, M. Hino, T. Kakiuchi, K. Okada, K. Tabayashi, T. Matsudo, Y. Yamana, I.H. Suzuki, Y. Tamenori, Chem. Phys. Lett. 392 (2004) 303.
[6] D.M.P. Holland, D.A. Shaw, I.C. Walker, I.J. McEwen, E. Aprà, M.F. Guest, J. Phys. B 38 (2005) 2047.
[7] E. Hudson, D.A. Shirley, M. Domke, G. Remmers, A. Puschmann, T. Mandell, C. Xue, G. Kaindl, Phys. Rev. A 47 (1993) 361.
[8] J.T. Francis, C.C. Turci, T. Tyliszczak, G.G.B. de Souza, N. Kosugi, A.P. Hitchcock, Phys. Rev. A 52 (1995) 4665.
[9] V.T. Nefedov, J. Struct. Chem. 11 (1970) 272.
[10] J.A. Sheehy, T.J. Gil, C.L. Winstead, R.E. Farren, P.W. Langhoff, J. Chem. Phys. 91 (1989) 1796.
[11] A. Kivimäki, J. Alvarez Ruiz, M. Coreno, M. Stankiewicz, G. Fronzoni, P. Decleva, Chem. Phys. 353 (2008) 202.
[12] K.C. Prince et al., J. Synchrotron Radiat. 5 (1998) 565.
[13] J.A.R. Samson, Z.X. He, L. Yin, G.N. Haddad, J. Phys. B 27 (1994) 887.
[14] N. Kosugi, J. Electr. Spectrosc. Relat. Phenom. 137–140 (2004) 335.
[15] E.J. Baerends, D.E. Ellis, P. Ros, Chem. Phys. 2 (1973) 41.
[16] C. Fonseca Guerra, J.G. Snijders, G. te Velde, E.J. Baerends, Theor. Chem. Acc. 99 (1998) 391.
[17] S.J.A. van Gisbergen, J.G. Snijders, E.J. Baerends, Comput. Phys. Commun. 118 (1999) 119.
[18] M.E. Casida, in: D.P. Chong (Ed.), Recent Advances in Density-Functional Methods, World Scientific, Singapore, 1995, p. 155.
[19] M. Stener, G. Fronzoni, M. de Simone, Chem. Phys. Lett. 373 (2003) 115.
[20] G. Fronzoni, M. Stener, P. Decleva, F. Wang, T. Ziegler, E. van Lenthe, E.J. Baerends, Chem. Phys. Lett. 416 (2005) 56.
[21] M. Stener, G. Fronzoni, P. Decleva, J. Chem. Phys. 122 (2005) 234301.
[22] M. Stener, D. Toffoli, G. Fronzoni, P. Decleva, J. Chem. Phys. 124 (2006) 114306.
[23] R. Van Leeuwen, E.J. Baerends, Phys. Rev. A 49 (1994) 2421.
[24] E. van Lenthe, E.J. Baerends, J. Comput. Chem. 24 (2003) 1142.
[25] G. Fronzoni, M. Stener, P. Decleva, M. de Simone, M. Coreno, P. Franceschi, K. Prince, C. Furlani, J. Phys. Chem. A 113 (2009) 2914.
[26] T.A. Ferrett, D.W. Lindle, P.A. Heimann, M.N. Piancastelli, P.H. Kobrin, H.G. Kerkhoff, U. Becker, W.D. Brewer, D.A. Shirley, J. Chem. Phys. 89 (1988) 4726.
[27] H. Nakamatsu, T. Mukoyama, H. Adachi, J. Chem. Phys. 95 (1991) 3167; H. Nakamatsu, T. Mukoyama, H. Adachi, Chem. Phys. 142 (1990) 221.
[28] G. Fronzoni, R. De Francesco, M. Stener, P. Decleva, J. Chem. Phys. 126 (2007) 134308.
[29] I.G. Eustatiu, T. Tyliszczak, A.P. Hitchcock, Chem. Phys. Lett. 300 (1999) 676.
[30] I.G. Eustatiu, J.T. Francis, T. Tyliszczak, C.C. Turci, A.L.D. Kilcoyne, A.P. Hitchcock, Chem. Phys. 257 (2000) 235.
[31] G. Fronzoni, M. Stener, S. Furlan, P. Decleva, Chem. Phys. 273 (2001) 117.
[32] Y. Sato, K. Ueda, H. Chiba, E. Shigemasa, A. Yagishita, Chem. Phys. Lett. 196 (1991) 475.
[33] A. Kivimäki, J. Álvarez Ruiz, P. Erman, P. Hatherly, E. Melero García, E. Rachlew, J. Rius I Riu, M. Stankiewicz, J. Phys. B 36 (2003) 781.
[34] M. Kitajima, M. Hoshino, M. Okamoto, T. Suzuki, H. Tanaka, Y. Shimizu, Y. Muramatsu, H. Chiba, K. Ueda, T. Hayaishi, M. Simon, M. Kimura, Phys. Rev. A 63 (2001) 050703(R).